



Sensor Selection for Aircraft Engine Performance Estimation and Gas Path Fault Diagnostics

Donald L. Simon
Glenn Research Center, Cleveland, Ohio

Aidan W. Rinehart
Vantage Partners, LLC, Brook Park, Ohio

NASA STI Program . . . in Profile

Since its founding, NASA has been dedicated to the advancement of aeronautics and space science. The NASA Scientific and Technical Information (STI) Program plays a key part in helping NASA maintain this important role.

The NASA STI Program operates under the auspices of the Agency Chief Information Officer. It collects, organizes, provides for archiving, and disseminates NASA's STI. The NASA STI Program provides access to the NASA Technical Report Server—Registered (NTRS Reg) and NASA Technical Report Server—Public (NTRS) thus providing one of the largest collections of aeronautical and space science STI in the world. Results are published in both non-NASA channels and by NASA in the NASA STI Report Series, which includes the following report types:

- **TECHNICAL PUBLICATION.** Reports of completed research or a major significant phase of research that present the results of NASA programs and include extensive data or theoretical analysis. Includes compilations of significant scientific and technical data and information deemed to be of continuing reference value. NASA counter-part of peer-reviewed formal professional papers, but has less stringent limitations on manuscript length and extent of graphic presentations.
- **TECHNICAL MEMORANDUM.** Scientific and technical findings that are preliminary or of specialized interest, e.g., “quick-release” reports, working papers, and bibliographies that contain minimal annotation. Does not contain extensive analysis.
- **CONTRACTOR REPORT.** Scientific and technical findings by NASA-sponsored contractors and grantees.
- **CONFERENCE PUBLICATION.** Collected papers from scientific and technical conferences, symposia, seminars, or other meetings sponsored or co-sponsored by NASA.
- **SPECIAL PUBLICATION.** Scientific, technical, or historical information from NASA programs, projects, and missions, often concerned with subjects having substantial public interest.
- **TECHNICAL TRANSLATION.** English-language translations of foreign scientific and technical material pertinent to NASA's mission.

For more information about the NASA STI program, see the following:

- Access the NASA STI program home page at <http://www.sti.nasa.gov>
- E-mail your question to help@sti.nasa.gov
- Fax your question to the NASA STI Information Desk at 757-864-6500
- Telephone the NASA STI Information Desk at 757-864-9658
- Write to:
NASA STI Program
Mail Stop 148
NASA Langley Research Center
Hampton, VA 23681-2199



Sensor Selection for Aircraft Engine Performance Estimation and Gas Path Fault Diagnostics

*Donald L. Simon
Glenn Research Center, Cleveland, Ohio*

*Aidan W. Rinehart
Vantage Partners, LLC, Brook Park, Ohio*

Prepared for
Turbo Expo 2015
sponsored by the the American Society of Mechanical Engineers (ASME)
Montreal, Quebec, Canada, June 15–19, 2015

National Aeronautics and
Space Administration

Glenn Research Center
Cleveland, Ohio 44135

Acknowledgments

This work was conducted under the NASA Aviation Safety Program, Vehicle Systems Safety Technologies Project.

Level of Review: This material has been technically reviewed by technical management.

Available from

NASA STI Program
Mail Stop 148
NASA Langley Research Center
Hampton, VA 23681-2199

National Technical Information Service
5285 Port Royal Road
Springfield, VA 22161
703-605-6000

This report is available in electronic form at <http://www.sti.nasa.gov/> and <http://ntrs.nasa.gov/>

Sensor Selection for Aircraft Engine Performance Estimation and Gas Path Fault Diagnostics

Donald L. Simon
National Aeronautics and Space Administration
Glenn Research Center
Cleveland, Ohio 44135

Aidan W. Rinehart
Vantage Partners, LLC
Brook Park, Ohio 44142

Abstract

This paper presents analytical techniques for aiding system designers in making aircraft engine health management sensor selection decisions. The presented techniques, which are based on linear estimation and probability theory, are tailored for gas turbine engine performance estimation and gas path fault diagnostics applications. They enable quantification of the performance estimation and diagnostic accuracy offered by different candidate sensor suites. For performance estimation, sensor selection metrics are presented for two types of estimators including a Kalman filter and a maximum *a posteriori* estimator. For each type of performance estimator, sensor selection is based on minimizing the theoretical sum of squared estimation errors in health parameters representing performance deterioration in the major rotating modules of the engine. For gas path fault diagnostics, the sensor selection metric is set up to maximize correct classification rate for a diagnostic strategy that performs fault classification by identifying the fault type that most closely matches the observed measurement signature in a weighted least squares sense. Results from the application of the sensor selection metrics to a linear engine model are presented and discussed. Given a baseline sensor suite and a candidate list of optional sensors, an exhaustive search is performed to determine the optimal sensor suites for performance estimation and fault diagnostics. For any given sensor suite, Monte Carlo simulation results are found to exhibit good agreement with theoretical predictions of estimation and diagnostic accuracies.

Introduction

Aircraft operators rely on engine performance estimation and gas path fault diagnostics to ensure the safe and efficient operation of their gas turbine engine assets. Performance estimation enables the estimation and trending of gradual performance deterioration that the engine will experience over time due to fouling, corrosion, and erosion of turbomachinery components. Gas path fault diagnostics enables the detection and isolation of gas path system faults affecting engine

performance, which are typically relatively rapid or abrupt in nature (Refs. 1 and 2). A notional illustration of the observed measurement shifts caused by gradual deterioration compared to an abrupt fault is shown in Figure 1.

Although performance estimation and gas path fault diagnostics typically apply different algorithmic approaches, both are conducted using the same engine sensor measurement data—primarily data acquired from the available engine control sensor suite. In general, adding additional engine sensors will improve performance estimation and diagnostic accuracy, but this does add to the overall engine life cycle cost. Therefore, the decision to add sensors should be made judiciously.

Several researchers have presented sensor selection approaches for engine health management applications. Mushini and Simon (no relation to the author) proposed a sensor selection approach for Kalman filter-based performance estimation applications (Ref. 3). In this work, a performance metric was defined as a function of the steady state error covariance and the cost of the selected sensors. Three separate metrics were considered for searching for the optimal sensor suite, including a random search, a genetic algorithm search, and an exhaustive search. The study by Mushini and Simon assumed that the estimation problem was over-determined (i.e., there are more sensors than unknown parameters to be estimated), which is usually not the case for engine performance estimation applications. Borguet and Léonard approached the problem of sensor selection for engine performance estimation within the scope of linear information theory (Ref. 4). They defined performance metrics based on the Fisher information matrix, and an exhaustive search was conducted to identify the best sensor suite. Sowers et al. introduced a systematic framework for automating sensor selection decisions for diagnostic applications. This framework enables incorporation of factors of merit commonly considered in the sensor selection process including diagnostic accuracy, diagnostic criticality, and cost (Ref. 5). The framework relies on the end user to specify the merit function used by the optimal search algorithm. Kamboukos et al. proposed sensor selection for performance

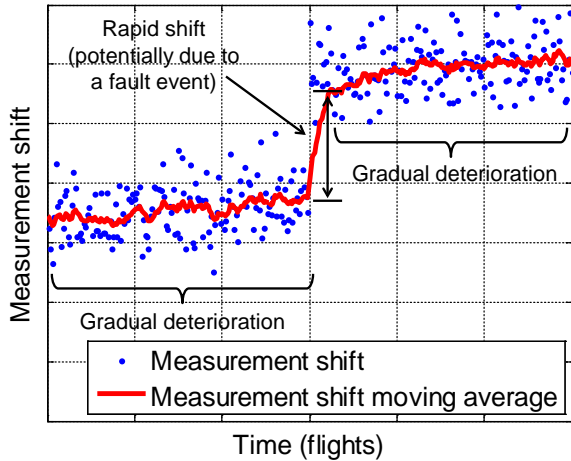


Figure 1.—Gradual versus rapid performance shifts.

estimation applications based on the condition number of the influence matrix that relates changes in health parameters to changes in sensed measurements (Ref. 6). Here, a determined health parameter estimation problem was considered where there are as many sensors as parameters to be estimated.

The contribution of this paper will be to introduce separate sensor selection metrics for performance estimation and fault diagnostic applications. In terms of performance estimation, the problem is assumed to be underdetermined (i.e., fewer sensors than unknown health parameters to be estimated), and two separate estimators will be considered—one applying a Kalman filter designed for processing dynamic sensed measurement information, and a second applying a maximum *a posteriori* estimator for processing quasi-steady-state measurement data. In terms of fault diagnostics, a single fault diagnostic strategy applying a weighted least squares hypothesis test will be considered.

The remainder of this paper is organized as follows. First, metrics are defined through analytical derivations of the performance estimation accuracy and gas path fault diagnostic accuracy based on linear system theory. These analytical functions can be directly used to theoretically predict the estimation or diagnostic accuracy offered by a given sensor suite. Next, example application of the sensor selection techniques is presented by applying the approaches to a linear engine model. Theoretically predicted results are calculated and compared against empirical results obtained through Monte Carlo simulation analysis. This is followed by discussions and conclusions.

Nomenclature

$A, A_{xh}, A_{xq}, B, B_{xh}, B_{xq}$, system matrices
 $C, C_{xh}, C_{xq}, D, L, M$
 CCR correct classification rate

| | |
|--------------------------|--|
| C-MAPSS40k | Commercial Modular Aero-Propulsion System Simulation 40k |
| D_M | Mahalanobis distance |
| FPR | false positive rate |
| H | influence coefficient matrix relating changes in health parameters to changes in sensed measurements |
| H_f | fault influence coefficient matrix relating faults to changes in sensed measurements |
| I | identity matrix |
| MAP | maximum <i>a posteriori</i> |
| N | number of fault types |
| PMC | probability of misclassification |
| P_h | health parameter covariance matrix |
| R | measurement noise covariance matrix |
| $SSEE$ | sum of squared estimation errors |
| T | fault detection threshold |
| TPR | true positive rate |
| V^* | transformation matrix relating h to q |
| $WSSE$ | weighted sum of squared errors |
| $WSSM$ | weighted sum of squared measurements |
| h | health parameter vector |
| f | fault vector |
| k | number of additional sensors to add |
| m | number of tuning parameters |
| n | Number of additional sensors to choose from |
| p | number of health parameters |
| q | reduced order tuning parameter vector |
| u | actuator command vector |
| v | measurement noise vector |
| $w_k, w_{h,k}, w_{xh,k}$ | process noise vectors |
| x | state vector |
| y | measurement vector |
| Γ | gamma function |
| γ | lower incomplete gamma function |
| ε | residual vector (estimate minus its expected value) |
| Φ | standard normal distribution function |
| λ | mean value of the $WSSM$ signal |
| μ_i | mean value of i^{th} sensed measurement |
| Subscripts | |
| a | fault type index |
| b | misclassified fault type index |
| k | sample index |
| xh | augmented state vector (x and h) |
| xq | reduced order state vector (x and q) |
| Superscripts | |
| \dagger | pseudo-inverse |
| $\hat{}$ | estimated value |
| \sim | error value |
| $\bar{}$ | mean value |

Operators

| | |
|------------------------|----------------------------|
| $E[\bullet]$ | expected value of argument |
| $\text{tr}\{\bullet\}$ | trace of a matrix |

Sensor Selection Metrics

As previously mentioned, aircraft engine performance estimation and gas path fault diagnostics pose different problem formulations. Analytical formulations of each are introduced below along with derivations of performance estimation and diagnostic accuracy for a given sensor suite. The performance estimation problem assumes the application of two separate estimators—a linear Kalman filter and a maximum *a posteriori* estimator, while the gas path fault diagnostic problem assumes the application of a single fault isolator applying a weighted least squares hypothesis test.

Kalman Filter-Based Health Parameter Estimation

In the aircraft engine community, Kalman filters are commonly applied for on-board performance estimation or post-flight analysis of full-flight streaming measurement data. In this subsection, Kalman filter health parameter estimation accuracy is discussed following a derivation previously introduced by Simon and Garg as part of an optimal tuner selection methodology for Kalman filter-based performance estimation applications (Ref. 7). This optimal tuner selection methodology is designed to minimize the Kalman mean squared estimation error in the parameters of interest when facing underdetermined estimation problems, but can readily be extended to also calculate the mean squared estimation error offered by different sensor suites, as was shown in Reference 8.

The formulation begins by considering the following discrete linear time-invariant state space equations representing engine dynamics about an operating point

$$\begin{aligned}\Delta x_{k+1} &= A\Delta x_k + B\Delta u_k + L\Delta h_k + w_k \\ \Delta y_k &= C\Delta x_k + D\Delta u_k + M\Delta h_k + v_k\end{aligned}\quad (1)$$

where k is the sample index, x is the vector of state variables, u is the vector of control inputs, and y is the vector of measured outputs. The vector h , where $h \in \mathbb{R}^p$, represents the engine health parameters, which induce shifts in other variables as the health parameters deviate from their nominal values. The Δ symbols denote parameter deviations relative to the linear operating point trim condition. The vectors w and v are uncorrelated zero-mean white noise input sequences. The

matrices A , B , C , D , L , and M are of appropriate dimensions. Through algebraic manipulation, Equation (1) can be rewritten such that h is concatenated with x to form an augmented state vector, x_{xh} , as shown in Equation (2). Since engine performance deterioration is very slowly evolving relative to other engine dynamics, h is here modeled without dynamics. Here, and throughout the remainder of this section, the Δ symbols are omitted for simplicity.

$$\begin{aligned}\begin{bmatrix} x_{k+1} \\ h_{k+1} \end{bmatrix} &= \underbrace{\begin{bmatrix} A & L \\ 0 & I \end{bmatrix}}_{A_{xh}} \underbrace{\begin{bmatrix} x_k \\ h_k \end{bmatrix}}_{x_{xh,k}} + \underbrace{\begin{bmatrix} B \\ 0 \end{bmatrix}}_{B_{xh}} u_k + \underbrace{\begin{bmatrix} w_k \\ w_{h,k} \end{bmatrix}}_{w_{xh,k}} \\ &= A_{xh}x_{xh,k} + B_{xh}u_k + w_{xh,k}\end{aligned}\quad (2)$$

$$\begin{aligned}y_k &= \underbrace{\begin{bmatrix} C & M \end{bmatrix}}_{C_{xh}} \underbrace{\begin{bmatrix} x_k \\ h_k \end{bmatrix}}_{x_{xh,k}} + Du_k + v_k \\ &= C_{xh}x_{xh,k} + Du_k + v_k\end{aligned}$$

The vector w_{xh} is zero-mean white noise associated with the augmented state vector, $[x^T \ h^T]^T$. w_{xh} consists of the original state process noise, w , concatenated with the process noise associated with the health parameter vector, w_h .

Once the h vector is appended to the state vector as shown in Equation (2), it may be directly estimated by applying a Kalman filter as long as the system is observable. However, the number of health parameters that can be estimated is limited to the number of sensors, the dimension of y (Ref. 9), and typically an aircraft gas turbine engine has fewer sensors than health parameters. To enable Kalman filter formulation for an underdetermined estimation problem, a reduced-order state space model is constructed. This is accomplished by defining a model tuning parameter vector, q , which is a linear combination of all health parameters, h , given by

$$q = V^*h \quad (3)$$

where $q \in \mathbb{R}^m$, $h \in \mathbb{R}^p$, $m < p$, and V^* is an $m \times p$ transformation matrix of rank m , which relates h to q . Given an estimate of q (i.e., \hat{q}), an approximation of the health parameter vector, \hat{h} , can be obtained as

$$\hat{h} = V^{*\dagger}\hat{q} \quad (4)$$

where $V^{*\dagger}$ is the pseudo-inverse of V^* . Substituting Equation (4) into Equation (2) yields the following reduced-order state space equations, which may be used to formulate a Kalman filter

$$\begin{aligned}
\underbrace{\begin{bmatrix} x_{k+1} \\ q_{k+1} \end{bmatrix}}_{x_{xq,k+1}} &= \underbrace{\begin{bmatrix} A & LV^{*\dagger} \\ 0 & I \end{bmatrix}}_{A_{xq}} \underbrace{\begin{bmatrix} x_k \\ q_k \end{bmatrix}}_{x_{xq,k}} + \underbrace{\begin{bmatrix} B \\ 0 \end{bmatrix}}_{B_{xq}} u_k + \underbrace{\begin{bmatrix} w_k \\ w_{q,k} \end{bmatrix}}_{w_{xq,k}} \\
&= A_{xq} x_{xq,k} + B_{xq} u_k + w_{xq,k} \\
&\quad (5) \\
y_k &= \underbrace{\begin{bmatrix} C & MV^{*\dagger} \\ & C_{xq} \end{bmatrix}}_{C_{xq}} \underbrace{\begin{bmatrix} x_k \\ q_k \end{bmatrix}}_{x_{xq,k}} + Du_k + v_k \\
&= C_{xq} x_{xq,k} + Du_k + v_k
\end{aligned}$$

The reduced-order equations introduced in Equation (5) will enable a Kalman filter to be formulated that can estimate the augmented state vector, $[x^T q^T]^T$. The resulting Kalman filter-produced tuner parameter vector estimate, \hat{q} , can be inserted into Equation (4) to produce an estimated health parameter vector, \hat{h} . However, this does not circumvent the underdetermined nature of the \hat{h} estimation problem, and the fact that the produced \hat{h} estimates will contain errors is unavoidable. However, estimation accuracy is directly dependent on the available sensor suite and the selection of the transformation matrix, V^* . This gives rise to an optimization problem of selecting the best sensor suite and the corresponding V^* that minimizes the estimation error in the parameters of interest. For a given sensor suite, an optimal iterative search can be conducted to select a V^* matrix that minimizes the theoretical mean sum of squared estimation errors (*SSEE*) in the parameters of interest

$$\arg \min_{V^* \in \mathbb{R}^{m \times p}} SSEE(V^*) \quad (6)$$

where the above statement indicates the V^* matrix that minimizes the *SSEE* function. Once V^* is obtained, it can be inserted into Equation (5) to construct the reduced-order state space equations. Here, it is important to emphasize that the V^* matrix and q vector are unique to each sensor suite considered. Therefore, Equation (6) is individually applied to each sensor suite, and the suite that provides the lowest *SSEE* is identified as optimal.

Due to page limitations, a complete derivation of the Kalman filter *SSEE* metric is not provided in this document. However, readers are referred to Reference 7 for this derivation. Some notable aspects regarding the derivation are that it focuses on linear Kalman filter estimation accuracy under steady-state operating conditions, and that the error of each estimated parameter comprises mean squared bias and variance terms. Additionally, the derivation incorporates user-specified *a priori* knowledge regarding the health parameter

covariance matrix reflecting the expected distribution in the health parameters to be estimated. While this paper will only consider Kalman filter health parameter estimation accuracy, the technique can be readily extended to optimize the estimation accuracy of any unmeasured performance parameters such as thrust, airflows, or metal temperatures.

Maximum A Posteriori Health Parameter Estimation

Maximum *a posteriori* (MAP) estimation is commonly applied for ground-based aircraft engine gas path analysis. It is based on quasi-steady-state engine snapshot measurements acquired in flight (Refs. 2 and 10). Unlike the Kalman filter, which is a recursive estimator designed to process dynamic measurement data, the MAP estimator provides a point estimate based on an assumed quasi-steady-state measurement process. The MAP estimator incorporates *a priori* knowledge regarding the distribution of the parameters to be estimated, which enables it to provide an estimate when facing underdetermined estimation problems. To introduce the MAP estimator, consider the following linear steady-state measurement process

$$\Delta y = H \Delta h + v \quad (7)$$

where H is an influence coefficient matrix that relates the effects of the health parameter vector changes, Δh , to changes (i.e., residuals) in the sensed measurement vector, Δy . Here, v , is zero-mean white noise with covariance R . As with the previously introduced Kalman filter equations, the Δ symbols denote parameter deviations relative to the operating point trim condition at which Equation (7) was generated. For simplicity, the Δ symbols are omitted throughout the remainder of this section on the MAP estimator and the terms y and h are used to indicate measurement and health parameter changes, respectively. The maximum *a posteriori* (MAP) estimator follows the closed form expression

$$\begin{aligned}
\hat{h} &= \underbrace{(P_h^{-1} + H^T R^{-1} H)^{-1} H^T R^{-1} y}_{G_h} \\
\hat{h} &= G_h y
\end{aligned} \quad (8)$$

where P_h is a matrix containing *a priori* knowledge of the expected health parameter covariance. As with the Kalman filter introduced above, the MAP estimator produces a biased estimate due to the underdetermined nature of the estimation problem. However, its accuracy depends on the available sensor suite, thus giving rise to a sensor selection problem. As with the Kalman filter, the MAP health parameter estimation error will be defined in terms of the sum of squared estimation errors (*SSEE*), which consists of the sum of two components: mean squared bias and variance, as defined below.

MAP Estimation Mean Squared Bias

The bias of an estimator is the expected difference between the estimator's estimated value and the true value of the parameter being estimated. For the MAP estimator, the estimated health parameter bias vector, \widetilde{h} , is defined as

$$\begin{aligned}
 \widetilde{h} &= E[\hat{h} - h] \\
 &= E\left[G_h y - h\right] \\
 &= E\left[G_h(Hh + v) - h\right] \\
 &= E[(G_h H - I)h + G_h v] \\
 &= (G_h H - I)E[h] + G_h E[v] \\
 &= (G_h H - I)h
 \end{aligned} \tag{9}$$

where the operator $E[\bullet]$ represents the expected value of the argument, and the expected value properties $E[h]=h$ and $E[v]=0$ are leveraged in Equation (9). The estimation error bias equation given in Equation (9) is a function of an arbitrary health parameter vector h . The mean sum of squared biases across a fleet of engines is given as

$$\begin{aligned}
 \widetilde{h}^2 &= E[\widetilde{h}^T \widetilde{h}] = E\left[\text{tr}\{\widetilde{h} \widetilde{h}^T\}\right] \\
 &= E\left[\text{tr}\{(G_h H - I)h h^T (G_h H - I)^T\}\right] \\
 &= \text{tr}\left\{(G_h H - I)E[h h^T](G_h H - I)^T\right\} \\
 &= \text{tr}\left\{(G_h H - I)P_h(G_h H - I)^T\right\}
 \end{aligned} \tag{10}$$

where $\text{tr}\{\bullet\}$ represents the trace (sum of the diagonal elements) of the matrix. Here, the $E[h h^T]$ reduces to the health parameter covariance matrix, P_h , which is leveraged in Equation (10).

MAP Estimation Variance

The variance of the MAP estimate is found by constructing the estimation covariance matrix, $P_{\hat{h}}$, which is defined as

$$P_{\hat{h}} = E\left[\underbrace{(\hat{h} - E[\hat{h}])}_{\varepsilon} \underbrace{(\hat{h} - E[\hat{h}])^T}_{\varepsilon}\right] \tag{11}$$

where the vector ε is the residual between \hat{h} and its expected value. By combining Equation (7) and Equation (8), ε can be written as

$$\begin{aligned}
 \varepsilon &= (\hat{h} - E[\hat{h}]) \\
 &= G_h y - E[G_h y] \\
 &= G_h(Hh + v) - E[G_h(Hh + v)] \\
 &= G_h H h + G_h v - G_h H \underbrace{E[h]}_h - G_h \underbrace{E[v]}_0 \\
 &= G_h v
 \end{aligned} \tag{12}$$

Then, by substituting Equation (12) into Equation (11) the covariance matrix of the MAP estimate becomes

$$\begin{aligned}
 P_{\hat{h}} &= E[\varepsilon \varepsilon^T] \\
 &= E[G_h v v^T G_h^T] \\
 &= G_h \underbrace{E[v v^T]}_R G_h^T \\
 &= G_h R G_h^T
 \end{aligned} \tag{13}$$

Diagonal elements of $P_{\hat{h}}$ will reflect the variance of individual health parameter estimates, while off diagonal elements reflect the covariance between estimates.

The overall sum of squared estimation errors (*SSEE*) can be obtained by combining the estimation mean squared bias and variance information as

$$SSEE(\hat{h}) = \text{tr}\{(G_h H - I)P_h(G_h H - I)^T\} + \text{tr}\{G_h R G_h^T\} \tag{14}$$

Mean squared bias and variance are equally weighted in the above equation. However, end users may weight them differently if they so choose.

Weighted Least Squares Single Fault Diagnostic Approach

Gas path fault diagnostics poses a different problem than that of performance estimation. Unlike performance deterioration, which is assumed to occur gradually and affect all health parameters simultaneously and somewhat independently, gas path faults are assumed to primarily occur abruptly and in isolation. In other words, it is rare to have multiple unrelated gas path system faults occurring simultaneously. Applying the single fault assumption transforms gas path fault diagnostics from an underdetermined to an over-determined estimation problem. This subsection will present a single fault isolator that applies a weighted least squares hypothesis test to diagnose faults. Additionally, the

accuracy offered by this diagnostic approach is analytically derived.

The fault diagnostic approach considered in this study, like the previously described MAP estimation approach, is ground-based, and designed to process snapshot engine measurements acquired in flight. To introduce the diagnostic approach, first assume the following linear steady-state sensor measurement process

$$\Delta\Delta y = H_f f + v \quad (15)$$

where $\Delta\Delta y$ is a vector of residuals reflecting recent shifts in engine sensor measurements, for example, the change measurements have undergone within the past one or two flights. Also shown in Equation (15) is f , a vector of gas path fault magnitudes, and H_f , a fault influence coefficient matrix relating fault magnitudes to sensor measurement residuals. Furthermore, v denotes zero-mean normally distributed sensor measurement noise of covariance R . The measurement residuals, $\Delta\Delta y$, are regularly updated as new snapshot data become available. They are referred to as “delta-delta” measurement shifts, as they will reflect fault induced shifts relative to the gradual deterioration induced shifts the engine has experienced up until the time of fault initiation (Ref. 2). Since faults are assumed to occur abruptly and cause relatively large measurement shifts, the $\Delta\Delta y$ residuals will be small in the case of no fault, and larger once a fault has occurred (see Fig. 1). For simplicity, the $\Delta\Delta$ symbols are omitted throughout the remainder of this section and the term y is used to indicate recent observed shifts in the sensor measurements. Given Equation (15), a fault detection and classification (isolation) approach can be formulated. Here, it is assumed that fault detection is performed by calculating and monitoring a weighted sum of squared measurement ($WSSM$) signal:

$$WSSM = y^T R^{-1} y \quad (16)$$

If the $WSSM$ signal exceeds an established detection threshold (T), a fault is assumed to be present and the diagnostic logic proceeds in attempting to isolate the most plausible single fault root cause for the fault. Here, fault classification is performed by applying a weighted least squares approach. Each possible gas path fault type is evaluated individually, and the hypothesized fault whose signature best matches the observed measurement residuals in a weighted least squares sense is classified as the fault. For the l^{th} fault type, the estimated fault magnitude is calculated as

$$\hat{f}_l = \left(H_{f,l}^T R^{-1} H_{f,l} \right)^{-1} H_{f,l}^T R^{-1} y \quad (17)$$

where $H_{f,l}$ is the column of the H_f matrix corresponding to the l^{th} fault type, and the scalar \hat{f}_l is the estimated magnitude of the l^{th} fault type that produces the best match of the observed vector of sensor measurement residuals, y , in a weighted least squares sense. The resulting \hat{f}_l estimate is then combined with $H_{f,l}$ to produce an estimated measurement residual vector, \hat{y}_l , for the l^{th} fault type:

$$\hat{y}_l = H_{f,l} \hat{f}_l \quad (18)$$

The difference between \hat{y}_l and y defines the estimation error vector for the l^{th} fault type, \tilde{y}_l , defined as

$$\tilde{y}_l = \hat{y}_l - y \quad (19)$$

The weighted sum of squared errors for the l^{th} hypothesized fault type is calculated as

$$WSSE_l = \tilde{y}_l^T R^{-1} \tilde{y}_l \quad (20)$$

After $WSSE$'s are calculated for each potential fault type they are compared, and the hypothesized fault type that produces the minimum $WSSE$ is classified as the fault cause. Theoretical predictions of fault detection and fault classification performance for the single fault isolator are given below.

Fault Detection Performance

For any diagnostic system, fault detection performance is directly related to the applied fault detection threshold. Larger thresholds will result in fewer false alarms in the absence of a fault (false positives), but will also result in fewer true detections when a fault is actually present (true positives), while the opposite is true for smaller thresholds. In order to facilitate a common basis of comparison, each sensor suite considered in this study applies a $WSSM$ fault detection threshold, T , necessary to achieve a user-specified target false positive rate (FPR). The FPR of a system monitoring a $WSSM$ signal for fault detection purposes can be approximated if it is assumed that all sensed measurements are independent in addition to being zero mean and normally distributed. With this simplification, the distribution of the $WSSM$ signal under the no-fault case will be the sum of the squares of k independent standard normal random variables, which is a chi square distribution with k degrees of freedom. The cumulative distribution function of a chi square distribution is given as (Ref. 11)

$$CDF(T, k) = \frac{\gamma\left(\frac{k}{2}, \frac{T}{2}\right)}{\Gamma\left(\frac{k}{2}\right)} \quad (21)$$

where $\Gamma(\cdot)$ is the gamma function and $\gamma(\cdot)$ is the lower incomplete gamma function. The above equation reflects the probability that a random sample of the *WSSM* signal is less than the threshold, T , when no fault is present (i.e., the true negative rate). Therefore, the false positive rate is given as

$$\begin{aligned} FPR(T, k) &= 1 - CDF(T, k) \\ &= 1 - \frac{\gamma\left(\frac{k}{2}, \frac{T}{2}\right)}{\Gamma\left(\frac{k}{2}\right)} \end{aligned} \quad (22)$$

When a fault occurs, the *WSSM* signal will be distributed as a non-central chi-squared distribution. This distribution will be a function of: 1) the detection threshold, T ; 2) the number of sensors, k ; and 3) the mean value of the *WSSM* signal. The mean value of the *WSSM* signal for a fault of given type and magnitude is defined as λ , where $\lambda = \sum_{i=1}^k \mu_i^2$, where μ_i is the mean value of the i^{th} sensor in the presence of the fault. Given this information, the true positive rate (*TPR*) can be calculated from the cumulative distribution function of the non-central chi-square distribution as (Ref. 11):

$$TPR(T, k, \lambda) = 1 - \left(\sum_{j=0}^{\infty} e^{-\lambda/2} \frac{(\lambda/2)^j}{j!} \frac{\gamma(j+k/2, T/2)}{\Gamma(j+k/2)} \right) \quad (23)$$

The above equation reflects the probability that a random sample of the *WSSM* signal is greater than the threshold, T , when a fault of magnitude λ is present. Given Equations (22) and (23), overall *FPR* and *TPR* for individual fault types can be approximated for any given sensor suite.

Fault Classification Performance

In this study an approximation of the theoretical misclassification rate is produced by considering the probability of misclassification between fault pair combinations (i.e., making the assumption that only two fault classes exist) given that a fault has been correctly detected. The two-class misclassification rate results across all fault pairs are then summed to estimate an overall misclassification rate. Calculating the two-class misclassification rate is readily

tractable compared to multi-class misclassification rate given three or more faults. While this simplification does not enable an exact calculation of the overall misclassification rate for a given fault type, it is effective for identifying fault pairs at high risk of misclassification. Let us consider a fault of a given type, a , and magnitude, f_a . From Equation (15), the expected sensed measurement vector under this condition becomes $y_a = H_{f,a} f_a$. The probability that a sensor measurement vector observation, y , collected when fault f_a is present is misclassified as fault type b (assumed to be of equivalent probability and resulting in equivalent sensor measurement covariance as fault type a) is given as (Ref. 12)

$$PMC_{b|a} = 1 - \Phi\left(\frac{1}{2} \cdot D_M\right) \quad (24)$$

where $PMC_{b|a}$ is the probability of misclassifying fault type a as b , Φ is the standard normal distribution function, and D_M is the Mahalanobis distance defined as

$$D_M = \min \left\{ \begin{array}{l} \sqrt{(y_a - y_b)^T R^{-1} (y_a - y_b)} \\ - \text{or} - \\ \sqrt{(y_a + y_b)^T R^{-1} (y_a + y_b)} \end{array} \right\} \quad (25)$$

The above expression accounts for the fact that the least squares estimation approach is able to produce bi-directional fault estimates of either a positive or negative magnitude. The sign that produces the minimum distance will have the largest contribution to the misclassification rate. In Equation (25), y_b is the expected sensor measurement vector for fault type b , scaled to be the same weighted length as y_a as shown in Equation (26)

$$y_b = H_b \frac{\sqrt{y_a^T R^{-1} y_a}}{\sqrt{H_b^T R^{-1} H_b}} \quad (26)$$

The above equations allow the probability of misclassification $PMC_{b|a}$ for each fault pair to be calculated. The overall probability of misclassification for fault type a can be approximated by summing all fault pair combinations:

$$PMC_a = \sum_{\substack{b=1 \\ b \neq a}}^N PMC_{b|a} \quad (27)$$

where N is the number of different fault types. Once PMC_a is obtained, an approximation of the correct classification rate (CCR) for fault type a of the considered fault magnitude can be found by combining the fault's *TPR* (given by Eq. (23)) and its *PMC* (given by Eq. (27)) as

$$CCR_a = TPR_a \times (1 - PMC_a) \quad (28)$$

The average CCR for the diagnostic system considering all fault types thus becomes

$$CCR = \sum_{a=1}^N \frac{CCR_a}{N} \quad (29)$$

where CCR_a is the correct classification rate for the a^{th} fault type, and N is the total number of fault types. The CCR shown in Equation (29) serves as a metric that can be used to estimate and compare the diagnostic performance offered by different candidate sensor suites.

Linear Turbofan Engine Model Example

In this section, an example application of the previously introduced metrics is given. This is done by applying the metrics to a linear point model and linear influence coefficient matrices extracted from the NASA Commercial Modular Aero-Propulsion System Simulation 40k (C-MAPSS40k) turbofan engine simulation (Ref. 13) at standard day sea level static conditions (i.e., air temperature = 59 °F, altitude = 0, and Mach = 0) and an intermediate power setting. The linear model, which is used for Kalman filter estimation, and is of the format shown in Equation (1), has seven state variables and three control inputs (actuator commands), as shown in Table 1, and ten health parameters, as shown in Table 2. The linear model has six baseline sensors, and four additional (optional) sensors, which are shown in Table 3 along with their corresponding standard deviations. Here, the sensor noise is assumed to be uncorrelated, zero-mean and normally distributed. The linear influence coefficient matrix to be used in MAP estimation (i.e., the H matrix given in Equation (7)), and the linear fault influence coefficient matrix to be used in gas path fault diagnostics (i.e., the H_f matrix given in Equation (15)), are generated from C-MAPSS40k at the same operating point as the linear model. However, these matrices are generated assuming that fan speed is held constant. As such, fan speed (Nf) is replaced by fuel flow (Wf) as one of the six baseline sensors when performing MAP estimation or gas path fault diagnostics.

The optional sensors shown in Table 3 are evaluated for the estimation accuracy or diagnostic improvement they provide if added individually or in combination to the baseline sensor suite. Given a set of n additional sensors to choose from, and a target number, k , of additional sensors, the total number of sensor suite combinations will be:

$$\binom{n}{k} = \frac{n!}{k!(n-k)!} \quad (30)$$

Therefore, the number of sensor combinations when adding 1, 2, 3, or 4 sensors to the baseline 6 sensors are:

- Baseline sensors 1 combination
- Baseline + 1 sensor ($n = 4, k = 1$) 4 combinations
- Baseline + 2 sensors ($n = 4, k = 2$) 6 combinations
- Baseline + 3 sensors ($n = 4, k = 3$) 4 combinations
- Baseline + 4 sensors ($n = 4, k = 4$) 1 combinations
- Total sensor combinations 16 combinations

TABLE 1.—STATE VARIABLES AND CONTROL INPUTS

| State variables (x) | Control inputs (u) |
|--------------------------------------|----------------------------|
| Nf – fan speed | Wf – fuel flow |
| Nc – core speed | VSV – variable stator vane |
| Hs_LPC – LPC metal temperature | VBV – variable bleed valve |
| Hs_HPC – HPC metal temperature | |
| Hs_burner – burner metal temperature | |
| Hs_HPT – HPT metal temperature | |
| Hs_LPT – LPT metal temperature | |

TABLE 2.—HEALTH PARAMETERS (h)

| | | |
|----|----------------|--|
| 1 | η_{FAN} | Fan efficiency |
| 2 | γ_{FAN} | Fan flow capacity |
| 3 | η_{LPC} | Low pressure compressor (LPC) efficiency |
| 4 | γ_{LPC} | Low pressure compressor (LPC) flow capacity |
| 5 | η_{HPC} | High pressure compressor (HPC) efficiency |
| 6 | γ_{HPC} | High pressure compressor (HPC) flow capacity |
| 7 | η_{HPT} | High pressure turbine (HPT) efficiency |
| 8 | γ_{HPT} | High pressure turbine (HPT) flow capacity |
| 9 | η_{LPT} | Low pressure turbine (LPT) efficiency |
| 10 | γ_{LPT} | Low pressure turbine (LPT) flow capacity |

TABLE 3.—SENSED OUTPUTS AND STANDARD DEVIATION AS PERCENT OF OPERATING POINT TRIM VALUES

| | Sensed output | Standard deviation |
|-------------------------------|-------------------------------------|--------------------|
| Baseline sensors | Nf ^a – fan speed (rpm) | 0.360 rpm |
| | Nc – core speed (rpm) | 1.23 rpm |
| | Ps30 – HPC exit static pressure | 0.333 psia |
| | T30 – HPC exit total temperature | 0.273 °R |
| | P50 – LPT exit total pressure | 0.021 psia |
| | T50 – LPT exit total temperature | 0.259 °R |
| Additional (optional) sensors | P14 – Bypass duct total pressure | 0.022 psia |
| | T14 – Bypass duct total temperature | 0.117 °R |
| | P25 – HPC inlet total pressure | 0.031 psia |
| | T25 – HPC inlet total temperature | 0.132 °R |

^aNote: For the MAP estimator and gas path fault diagnostics, fan speed (Nf) serves as the engine power reference parameter and is replaced in the list of six baseline sensors by fuel flow (Wf), which has a standard deviation of 9.03 pounds per hour (pph)

The subsections below will present and discuss results from the application of the sensor selection metrics for performance estimation and gas path fault diagnostics.

Sensor Selection for Performance Estimation

Performance estimation accuracy is assessed based on the health parameter mean squared estimation error offered by different sensor suites. The linear engine model contains 10 health parameters as shown in Table 2, which represent efficiency and flow capacity scalars associated with each major rotating module of the engine. In this study, deviations in all health parameters are assumed to be uncorrelated, and randomly shifted from their trim conditions with a standard deviation of ± 2 percent. Since a parameter's variance is equal to its standard deviation squared, the health parameter covariance matrix, P_h , is defined as a diagonal matrix with all diagonal elements equal to 4.0. The subsections below will present health parameter estimation results first assuming application of a Kalman filter estimator and then the MAP estimator.

Kalman Filter Sensor Selection Results

For each of the 16 candidate sensor suites, the Kalman filter *SSEE* metric shown in Equation (6) is applied to calculate the theoretical health parameter *SSEE* offered by each of the 16 candidate sensor suites. Additionally, a Monte Carlo simulation analysis is conducted to verify the theoretically predicted results. This is based on 200 health parameter vector combinations randomly selected in accordance with the defined health parameter covariance matrix, P_h . These random health parameter vectors and random measurement noise, v , are substituted into Equation (1) to produce sensed measurement test cases used for Monte Carlo evaluation. The resulting mean squared estimation error results are shown in Table 4. The top half of the table shows theoretically predicted results while the bottom half shows results obtained via the Monte Carlo simulation analysis. Each row corresponds to one of the 16 candidate sensor suites. In the cases of Baseline + 1, +2, or +3 optional sensors, the sensor suite that provides the minimum *SSEE* is highlighted in bold font. In general, adding sensors reduces the *SSEE*. The results also show that specific additional sensors are highly beneficial in improving the estimation accuracy of individual health parameters. For example, adding sensors such as P14 or T14 improves the estimation accuracy of fan efficiency (η_{FAN}) and fan flow capacity (γ_{FAN}), while adding P25 improves estimation accuracy of LPC flow capacity (γ_{LPC}). It is also encouraging to note that the theoretical and simulation results exhibit good agreement. The overall estimation accuracy is very similar and the combination of sensors identified as optimal is identical (theoretical vs. Monte Carlo simulation) for each candidate number of sensors. Minor differences between theoretical and

Monte Carlo results are likely due to the number of Monte Carlo trials conducted. If the number of trials were increased, the differences between analytical and simulation results should diminish. Based on this analysis, the sensor selection decisions for Kalman filter estimation accuracy would be:

- Baseline + 1 sensor, choose: T25
- Baseline + 2 sensors, choose: T25 and P25
- Baseline + 3 sensors, choose: T25, P25, and P14

MAP Estimator Sensor Selection Results

Next, sensor selection is conducted assuming that a MAP estimator is applied for health parameter estimation. Here, the metric previously introduced in Equation (14) is used to theoretically predict the health parameter *SSEE* accuracy offered by each of the candidate sensor suites. Additionally, a Monte Carlo simulation study is performed to verify the theoretical results. Here, 400,000¹ health parameter vectors are randomly generated in accordance with P_h . These health parameters along with random sensor measurement noise are substituted into Equation (7) to produce sensed measurement test cases, which are then processed to produce health parameter estimates using Equation (8). The resulting theoretical and Monte Carlo simulation health parameter mean squared estimation errors are shown in Table 5. Here, the theoretical and Monte Carlo simulation results exhibit very good agreement, which is expected given the large number of Monte Carlo trials runs. The sensor suites identified as optimal for the MAP estimator agree with those previously identified in Table 4 for the Kalman filter. Furthermore, the mean squared estimation errors of individual health parameters and the overall health parameter *SSEE* for most sensor suites exhibit fairly good agreement between the MAP estimator and the Kalman filter. This is not unexpected since both estimators are designed to minimize the mean sum of squared estimation errors, and in this study both incorporate the same *a priori* knowledge regarding health parameter covariance, P_h , and make the same assumptions regarding sensor measurement covariance, R .

¹ The disparity in the number of Monte Carlo trials conducted for the MAP estimator versus the Kalman filter is due to the nature of the two estimators. The MAP estimator only requires a single steady-state sample for each random health parameter vector considered. Conversely, the Kalman filter, which is a dynamic recursive estimator, requires a sufficient quantity of measurement data at each health condition to ensure convergence to a steady-state solution. This limited the practical number of Monte Carlo trials for the Kalman filter.

TABLE 4.—KALMAN FILTER PERFORMANCE ESTIMATION ACCURACY

| No. sensors | Sensors added to baseline | | | | Theoretical Health Parameter Mean Squared Estimation Errors (% squared) | | | | | | | | | | |
|-------------|---------------------------|-----|-----|-----|---|----------------|--------------|----------------|--------------|----------------|--------------|----------------|--------------|----------------|--------------|
| | P14 | T14 | P25 | T25 | η_{FAN} | γ_{FAN} | η_{LPC} | γ_{LPC} | η_{HPC} | γ_{HPC} | η_{HPT} | γ_{HPT} | η_{LPT} | γ_{LPT} | SSEE |
| 6 | | | | | 2.53 | 1.66 | 3.34 | 3.07 | 0.26 | 1.51 | 0.95 | 0.04 | 1.00 | 2.85 | 17.21 |
| 7 | x | | | | 0.23 | 0.15 | 3.43 | 3.29 | 0.25 | 1.47 | 0.96 | 0.04 | 1.02 | 2.83 | 13.66 |
| 7 | | x | | | 0.17 | 0.20 | 3.47 | 3.22 | 0.26 | 1.48 | 0.95 | 0.04 | 1.01 | 3.01 | 13.81 |
| 7 | | | x | | 2.54 | 1.67 | 3.23 | 0.05 | 0.26 | 0.70 | 0.83 | 0.04 | 0.86 | 2.65 | 12.83 |
| 7 | | | | x | 2.50 | 1.65 | 1.94 | 0.69 | 0.22 | 1.29 | 0.80 | 0.04 | 0.83 | 2.62 | 12.58 |
| 8 | x | x | | | 0.15 | 0.15 | 9.09 | 0.34 | 0.74 | 2.25 | 1.52 | 0.04 | 1.62 | 6.54 | 22.45 |
| 8 | x | | x | | 0.23 | 0.15 | 3.33 | 0.05 | 0.27 | 0.73 | 0.82 | 0.04 | 0.86 | 2.67 | 9.14 |
| 8 | x | | | x | 0.24 | 0.15 | 1.94 | 0.69 | 0.22 | 1.29 | 0.79 | 0.04 | 0.82 | 2.60 | 8.78 |
| 8 | | x | x | | 0.13 | 0.16 | 3.83 | 0.05 | 0.31 | 0.82 | 0.94 | 0.04 | 0.99 | 3.18 | 10.44 |
| 8 | | x | | x | 0.14 | 0.17 | 2.07 | 0.74 | 0.23 | 1.37 | 0.82 | 0.04 | 0.87 | 2.82 | 9.27 |
| 8 | | | x | x | 2.51 | 1.66 | 0.03 | 0.05 | 0.01 | 0.06 | 0.80 | 0.04 | 0.83 | 2.64 | 8.60 |
| 9 | x | x | x | | 0.16 | 0.15 | 3.43 | 0.05 | 0.27 | 0.74 | 0.99 | 0.04 | 1.05 | 3.19 | 10.07 |
| 9 | x | x | | x | 0.16 | 0.16 | 0.64 | 0.27 | 0.08 | 0.44 | 0.80 | 0.04 | 0.84 | 2.72 | 6.13 |
| 9 | x | | x | x | 0.24 | 0.15 | 0.03 | 0.05 | 0.01 | 0.06 | 0.79 | 0.04 | 0.83 | 2.61 | 4.79 |
| 9 | | x | x | x | 0.14 | 0.17 | 0.03 | 0.05 | 0.01 | 0.06 | 0.81 | 0.04 | 0.85 | 2.80 | 4.95 |
| 10 | x | x | x | x | 0.16 | 0.16 | 0.02 | 0.05 | 0.01 | 0.06 | 0.70 | 0.04 | 0.76 | 2.51 | 4.47 |
| No. sensors | Sensors added to baseline | | | | Monte Carlo Health Parameter Mean Squared Estimation Errors (% squared) | | | | | | | | | | |
| | P14 | T14 | P25 | T25 | η_{FAN} | γ_{FAN} | η_{LPC} | γ_{LPC} | η_{HPC} | γ_{HPC} | η_{HPT} | γ_{HPT} | η_{LPT} | γ_{LPT} | SSEE |
| 6 | | | | | 2.26 | 1.48 | 3.48 | 2.90 | 0.28 | 1.55 | 1.06 | 0.04 | 1.14 | 3.18 | 17.35 |
| 7 | x | | | | 0.23 | 0.15 | 3.52 | 2.95 | 0.27 | 1.46 | 1.04 | 0.04 | 1.11 | 3.17 | 13.94 |
| 7 | | x | | | 0.17 | 0.20 | 3.48 | 3.18 | 0.27 | 1.52 | 1.08 | 0.04 | 1.14 | 3.37 | 14.44 |
| 7 | | | x | | 2.29 | 1.51 | 3.34 | 0.05 | 0.27 | 0.73 | 0.99 | 0.04 | 1.05 | 2.92 | 13.19 |
| 7 | | | | x | 2.26 | 1.49 | 1.99 | 0.70 | 0.23 | 1.33 | 0.91 | 0.04 | 0.96 | 2.98 | 12.90 |
| 8 | x | x | | | 0.15 | 0.15 | 8.16 | 0.87 | 0.74 | 3.04 | 1.77 | 0.04 | 1.89 | 6.92 | 23.74 |
| 8 | x | | x | | 0.23 | 0.15 | 3.46 | 0.05 | 0.28 | 0.75 | 0.98 | 0.04 | 1.03 | 2.97 | 9.94 |
| 8 | x | | | x | 0.24 | 0.15 | 2.03 | 0.72 | 0.23 | 1.35 | 0.90 | 0.04 | 0.94 | 3.00 | 9.60 |
| 8 | | x | x | | 0.13 | 0.16 | 3.91 | 0.05 | 0.31 | 0.84 | 1.14 | 0.04 | 1.21 | 3.67 | 11.47 |
| 8 | | x | | x | 0.15 | 0.17 | 2.05 | 0.73 | 0.23 | 1.36 | 0.93 | 0.04 | 0.98 | 3.20 | 9.84 |
| 8 | | | x | x | 2.30 | 1.52 | 0.03 | 0.05 | 0.01 | 0.06 | 0.91 | 0.04 | 0.96 | 3.04 | 8.90 |
| 9 | x | x | x | | 0.16 | 0.15 | 3.30 | 0.05 | 0.26 | 0.71 | 1.20 | 0.04 | 1.28 | 4.52 | 11.66 |
| 9 | x | x | | x | 0.16 | 0.15 | 0.84 | 0.34 | 0.10 | 0.57 | 0.93 | 0.04 | 0.98 | 3.18 | 7.29 |
| 9 | x | | x | x | 0.24 | 0.15 | 0.03 | 0.05 | 0.01 | 0.06 | 0.91 | 0.04 | 0.95 | 3.03 | 5.45 |
| 9 | | x | x | x | 0.14 | 0.17 | 0.03 | 0.05 | 0.01 | 0.06 | 0.95 | 0.04 | 1.00 | 3.30 | 5.75 |
| 10 | x | x | x | x | 0.16 | 0.15 | 0.02 | 0.05 | 0.01 | 0.06 | 0.80 | 0.04 | 0.86 | 2.84 | 4.98 |

TABLE 5.—MAP ESTIMATOR PERFORMANCE ESTIMATION ACCURACY

| No. sensors | Sensors added to baseline | | | | Theoretical Health Parameter Mean Squared Estimation Errors (%squared) | | | | | | | | | | |
|-------------|---------------------------|-----|-----|-----|--|----------------|--------------|----------------|--------------|----------------|--------------|----------------|--------------|----------------|--------------|
| | P14 | T14 | P25 | T25 | η_{FAN} | γ_{FAN} | η_{LPC} | γ_{LPC} | η_{HPC} | γ_{HPC} | η_{HPT} | γ_{HPT} | η_{LPT} | γ_{LPT} | SSEE |
| 6 | | | | | 2.45 | 1.64 | 2.81 | 3.09 | 0.27 | 1.35 | 0.88 | 0.04 | 1.06 | 2.78 | 16.35 |
| 7 | x | | | | 0.48 | 0.15 | 2.81 | 3.08 | 0.27 | 1.34 | 0.88 | 0.04 | 1.04 | 2.78 | 12.86 |
| 7 | | x | | | 1.12 | 1.23 | 2.81 | 3.07 | 0.27 | 1.34 | 0.88 | 0.03 | 1.02 | 2.78 | 14.54 |
| 7 | | | x | | 2.45 | 1.64 | 2.75 | 0.04 | 0.27 | 0.91 | 0.75 | 0.04 | 0.90 | 2.62 | 12.36 |
| 7 | | | | x | 2.45 | 1.64 | 1.92 | 0.64 | 0.22 | 1.31 | 0.71 | 0.04 | 0.86 | 2.57 | 12.36 |
| 8 | x | x | | | 0.15 | 0.14 | 2.81 | 3.04 | 0.27 | 1.33 | 0.87 | 0.02 | 0.97 | 2.77 | 12.38 |
| 8 | x | | x | | 0.48 | 0.15 | 2.75 | 0.04 | 0.27 | 0.90 | 0.74 | 0.03 | 0.89 | 2.62 | 8.87 |
| 8 | x | | | x | 0.48 | 0.15 | 1.92 | 0.63 | 0.22 | 1.31 | 0.71 | 0.03 | 0.85 | 2.57 | 8.87 |
| 8 | | x | x | | 1.12 | 1.23 | 2.75 | 0.04 | 0.27 | 0.90 | 0.74 | 0.03 | 0.86 | 2.61 | 10.55 |
| 8 | | x | | x | 1.12 | 1.23 | 1.92 | 0.63 | 0.22 | 1.31 | 0.71 | 0.03 | 0.82 | 2.57 | 10.55 |
| 8 | | | x | x | 2.45 | 1.64 | 0.02 | 0.04 | 0.01 | 0.05 | 0.71 | 0.04 | 0.86 | 2.57 | 8.40 |
| 9 | x | x | x | | 0.15 | 0.14 | 2.75 | 0.02 | 0.27 | 0.89 | 0.74 | 0.02 | 0.80 | 2.61 | 8.39 |
| 9 | x | x | | x | 0.15 | 0.14 | 1.92 | 0.61 | 0.22 | 1.29 | 0.70 | 0.02 | 0.76 | 2.56 | 8.39 |
| 9 | x | | x | x | 0.48 | 0.15 | 0.02 | 0.04 | 0.01 | 0.05 | 0.71 | 0.03 | 0.85 | 2.57 | 4.91 |
| 9 | | x | x | x | 1.12 | 1.23 | 0.02 | 0.04 | 0.01 | 0.05 | 0.71 | 0.03 | 0.82 | 2.57 | 6.59 |
| 10 | x | x | x | x | 0.15 | 0.14 | 0.02 | 0.02 | 0.01 | 0.03 | 0.70 | 0.02 | 0.76 | 2.56 | 4.43 |

| No. sensors | Sensors added to baseline | | | | Monte Carlo Health Parameter Mean Squared Estimation Errors (%squared) | | | | | | | | | | |
|-------------|---------------------------|-----|-----|-----|--|----------------|--------------|----------------|--------------|----------------|--------------|----------------|--------------|----------------|--------------|
| | P14 | T14 | P25 | T25 | η_{FAN} | γ_{FAN} | η_{LPC} | γ_{LPC} | η_{HPC} | γ_{HPC} | η_{HPT} | γ_{HPT} | η_{LPT} | γ_{LPT} | SSEE |
| 6 | | | | | 2.46 | 1.64 | 2.81 | 3.10 | 0.27 | 1.34 | 0.88 | 0.04 | 1.06 | 2.78 | 16.36 |
| 7 | x | | | | 0.48 | 0.15 | 2.81 | 3.09 | 0.27 | 1.33 | 0.88 | 0.04 | 1.04 | 2.78 | 12.86 |
| 7 | | x | | | 1.13 | 1.23 | 2.81 | 3.08 | 0.27 | 1.34 | 0.88 | 0.03 | 1.02 | 2.78 | 14.55 |
| 7 | | | x | | 2.46 | 1.64 | 2.75 | 0.04 | 0.27 | 0.91 | 0.75 | 0.04 | 0.90 | 2.62 | 12.37 |
| 7 | | | | x | 2.46 | 1.64 | 1.91 | 0.64 | 0.22 | 1.31 | 0.71 | 0.04 | 0.86 | 2.57 | 12.36 |
| 8 | x | x | | | 0.15 | 0.14 | 2.81 | 3.05 | 0.27 | 1.32 | 0.87 | 0.02 | 0.97 | 2.77 | 12.38 |
| 8 | x | | x | | 0.48 | 0.15 | 2.75 | 0.04 | 0.27 | 0.90 | 0.74 | 0.03 | 0.89 | 2.62 | 8.86 |
| 8 | x | | | x | 0.48 | 0.15 | 1.91 | 0.63 | 0.22 | 1.30 | 0.71 | 0.03 | 0.85 | 2.57 | 8.86 |
| 8 | | x | x | | 1.12 | 1.23 | 2.75 | 0.04 | 0.27 | 0.90 | 0.74 | 0.03 | 0.86 | 2.62 | 10.55 |
| 8 | | x | | x | 1.12 | 1.23 | 1.91 | 0.63 | 0.22 | 1.30 | 0.71 | 0.03 | 0.82 | 2.57 | 10.54 |
| 8 | | | x | x | 2.46 | 1.64 | 0.02 | 0.04 | 0.01 | 0.05 | 0.71 | 0.04 | 0.86 | 2.57 | 8.41 |
| 9 | x | x | x | | 0.15 | 0.14 | 2.75 | 0.02 | 0.27 | 0.88 | 0.74 | 0.02 | 0.80 | 2.61 | 8.38 |
| 9 | x | x | | x | 0.15 | 0.14 | 1.91 | 0.61 | 0.22 | 1.29 | 0.70 | 0.02 | 0.76 | 2.56 | 8.38 |
| 9 | x | | x | x | 0.48 | 0.15 | 0.02 | 0.04 | 0.01 | 0.05 | 0.71 | 0.03 | 0.85 | 2.57 | 4.91 |
| 9 | | x | x | x | 1.12 | 1.23 | 0.02 | 0.04 | 0.01 | 0.05 | 0.71 | 0.03 | 0.82 | 2.57 | 6.60 |
| 10 | x | x | x | x | 0.15 | 0.14 | 0.02 | 0.02 | 0.01 | 0.03 | 0.70 | 0.02 | 0.76 | 2.56 | 4.43 |

Gas Path Fault Diagnostics Sensor Selection Results

For the gas path fault diagnostics sensor selection problem setup, it is assumed that the engine may encounter eight different gas path fault types consisting of turbomachinery faults (implemented via health parameter perturbations) and actuator biases. The eight faults along with the parameter perturbations applied within C-MAPSS40k to generate the fault influence coefficient matrix are shown in Table 6. For this study, all faults are assumed to occur in isolation and to be of equivalent probability of occurrence.

TABLE 6.—GAS PATH FAULTS

| Fault ID | Fault type | Health parameters and actuator biases |
|----------|------------|---|
| 1 | Fan fault | $\eta_{FAN} = -1\%$, $\gamma_{FAN} = -2\%$ |
| 2 | LPC fault | $\eta_{LPC} = -1\%$, $\gamma_{LPC} = -2\%$ |
| 3 | HPC fault | $\eta_{HPC} = -1\%$, $\gamma_{HPC} = -2\%$ |
| 4 | HPT fault | $\eta_{HPT} = -2\%$, $\gamma_{HPT} = +1\%$ |
| 5 | LPT fault | $\eta_{LPT} = -2\%$, $\gamma_{LPT} = +1\%$ |
| 6 | Wf bias | Wf bias = -2% |
| 7 | VSV bias | VSV bias = -1° stroke |
| 8 | VBV bias | VBV bias = $+20\%$ |

For each of the 16 candidate sensor suites, the correct classification rate metric given in Equation (29) is applied to calculate the theoretical correct classification rate offered by each candidate sensor suite. In making this assessment, the applied *WSSM* signal fault detection threshold is set to give a theoretical false positive rate of 0.01 (1 percent) as defined via Equation (22). This threshold will change based on the number of sensors included in each candidate sensor suite. Additionally, a Monte Carlo simulation analysis was conducted to verify the theoretically predicted CCR results. This is done using Equation (15) to generate 80,000 no fault cases and 10,000 fault cases for each individual fault type, all

corrupted by random measurement noise, v . This data set is then analyzed by applying the single fault diagnostic logic shown in Equations (16)-(20) to detect and classify the occurrence of any faults. Initial diagnostic analysis revealed that even the baseline 6 sensor measurement suite performed extremely well in diagnosing the gas path faults considered. Therefore, in order to present a more interesting sensor selection problem, the sensor measurement noise was increased by a factor of four and the diagnostic assessment was repeated. The ensuing correct classification rate results are shown in Table 7. The top half of the table shows theoretically predicted results while the bottom half shows

TABLE 7.—GAS PATH FAULT DIAGNOSTIC ACCURACY

| No. sensors | Sensors added to baseline | | | | Theoretical Correct Classification Rate (CCR) % | | | | | | | | | |
|-------------|---------------------------|----------|----------|----------|---|-------------|--------------|--------------|--------------|-------------|-------------|-------------|-------------|-------------|
| | P14 | T14 | P25 | T25 | Fan | LPC | HPC | HPT | LPT | Wf | VSV | VBV | No Fault | Fault CCR |
| 6 | | | | | 73.3 | 74.4 | 99.2 | 100.0 | 98.8 | 92.1 | 60.6 | 78.4 | 99.0 | 84.6 |
| 7 | x | | | | 80.6 | 74.6 | 99.2 | 100.0 | 99.8 | 90.6 | 60.7 | 78.6 | 99.0 | 85.5 |
| 7 | | x | | | 81.6 | 75.2 | 99.2 | 100.0 | 99.9 | 90.6 | 60.8 | 79.5 | 99.0 | 85.8 |
| 7 | | | x | | 76.3 | 87.1 | 99.9 | 100.0 | 98.8 | 90.6 | 70.4 | 88.8 | 99.0 | 89.0 |
| 7 | | | | x | 77.0 | 94.2 | 99.9 | 100.0 | 98.8 | 90.6 | 73.3 | 98.8 | 99.0 | 91.6 |
| 8 | x | x | | | 86.3 | 75.4 | 99.2 | 100.0 | 100.0 | 89.0 | 60.7 | 79.7 | 99.0 | 86.3 |
| 8 | x | | x | | 82.9 | 87.2 | 99.9 | 100.0 | 99.8 | 89.1 | 70.1 | 88.9 | 99.0 | 89.7 |
| 8 | x | | | x | 83.5 | 94.3 | 99.9 | 100.0 | 99.8 | 89.1 | 72.9 | 98.8 | 99.0 | 92.3 |
| 8 | | x | x | | 83.8 | 87.6 | 99.9 | 100.0 | 99.9 | 89.1 | 70.1 | 89.3 | 99.0 | 90.0 |
| 8 | | x | | x | 84.4 | 94.3 | 99.9 | 100.0 | 99.9 | 89.1 | 72.9 | 98.8 | 99.0 | 92.4 |
| 8 | | | x | x | 77.5 | 95.9 | 99.9 | 100.0 | 98.8 | 89.1 | 76.3 | 98.8 | 99.0 | 92.0 |
| 9 | x | x | x | | 88.0 | 87.7 | 99.9 | 100.0 | 100.0 | 87.5 | 69.7 | 89.4 | 99.0 | 90.3 |
| 9 | x | x | | x | 88.4 | 94.4 | 99.9 | 100.0 | 100.0 | 87.5 | 72.4 | 98.8 | 99.0 | 92.7 |
| 9 | x | | x | x | 83.9 | 95.9 | 99.9 | 100.0 | 99.8 | 87.5 | 75.7 | 98.8 | 99.0 | 92.7 |
| 9 | | x | x | x | 84.7 | 96.0 | 99.9 | 100.0 | 99.9 | 87.5 | 75.8 | 98.8 | 99.0 | 92.8 |
| 10 | x | x | x | x | 88.7 | 96.0 | 99.9 | 100.0 | 100.0 | 86.0 | 75.2 | 98.8 | 99.0 | 93.1 |
| No. sensors | Sensors added to baseline | | | | Monte Carlo Correct Classification Rate (CCR)% | | | | | | | | | |
| | P14 | T14 | P25 | T25 | Fan | LPC | HPC | HPT | LPT | Wf | VSV | VBV | No Fault | Fault CCR |
| 6 | | | | | 77.3 | 79.2 | 99.3 | 100.0 | 98.8 | 92.1 | 78.1 | 82.5 | 99.0 | 88.4 |
| 7 | x | | | | 83.7 | 79.5 | 99.3 | 100.0 | 99.8 | 90.5 | 77.2 | 82.5 | 99.0 | 89.1 |
| 7 | | x | | | 83.9 | 80.0 | 99.3 | 100.0 | 99.8 | 90.4 | 77.1 | 82.9 | 99.0 | 89.2 |
| 7 | | | x | | 77.3 | 87.8 | 99.9 | 100.0 | 98.8 | 90.4 | 79.6 | 89.3 | 99.0 | 90.4 |
| 7 | | | | x | 77.7 | 94.7 | 100.0 | 100.0 | 98.8 | 90.3 | 80.4 | 98.9 | 98.9 | 92.6 |
| 8 | x | x | | | 87.8 | 80.2 | 99.3 | 100.0 | 100.0 | 89.1 | 76.3 | 83.1 | 99.0 | 89.5 |
| 8 | x | | x | | 84.0 | 88.1 | 99.9 | 100.0 | 99.8 | 89.1 | 78.7 | 89.3 | 99.0 | 91.1 |
| 8 | x | | | x | 84.1 | 94.7 | 100.0 | 100.0 | 99.8 | 89.0 | 79.4 | 98.9 | 98.9 | 93.2 |
| 8 | | x | x | | 84.0 | 88.6 | 99.9 | 100.0 | 99.8 | 89.0 | 78.5 | 89.6 | 99.0 | 91.2 |
| 8 | | x | | x | 84.3 | 94.8 | 100.0 | 100.0 | 99.8 | 89.0 | 79.6 | 99.0 | 99.0 | 93.3 |
| 8 | | | x | x | 77.5 | 96.0 | 100.0 | 100.0 | 98.8 | 88.9 | 80.6 | 98.9 | 99.0 | 92.6 |
| 9 | x | x | x | | 88.1 | 88.7 | 99.9 | 100.0 | 100.0 | 87.5 | 77.9 | 89.7 | 99.0 | 91.5 |
| 9 | x | x | | x | 88.3 | 94.8 | 100.0 | 100.0 | 100.0 | 87.7 | 78.8 | 99.0 | 99.0 | 93.5 |
| 9 | x | | x | x | 84.2 | 96.0 | 100.0 | 100.0 | 99.8 | 87.5 | 80.0 | 98.9 | 99.0 | 93.3 |
| 9 | | x | x | x | 84.3 | 96.1 | 100.0 | 100.0 | 99.8 | 87.4 | 80.0 | 99.0 | 99.0 | 93.3 |
| 10 | x | x | x | x | 88.3 | 96.1 | 100.0 | 100.0 | 100.0 | 86.0 | 79.3 | 99.0 | 99.0 | 93.6 |

results obtained via the Monte Carlo simulation analysis. Here, the theoretical results slightly underpredict the correct classification rates found via Monte Carlo analysis. This is due to the simplification made in deriving the theoretical correct classification rate, which essentially establishes a theoretical lower bound on this rate. Based on the theoretical analysis, the sensor selection decisions for gas path fault diagnostics would be:

- Baseline + 1 sensor, choose: T25
- Baseline + 2 sensors, choose: T25 and T14
- Baseline + 3 sensors, choose: T25, T14, and P25

The Monte Carlo simulation analysis shows the same optimal sensor suites except for the Baseline + 3 sensor case, where P14 would be substituted in place of P25.

Discussion

The sensor selection metrics introduced in this paper were shown to perform well in identifying optimal sensor suites from a performance estimation and diagnostic accuracy perspective. Although not specifically shown in this paper, the resulting sensor suites identified to be optimal are expected to change if different assumptions are made regarding the design inputs such as sensor measurement noise, health parameter covariance, fault types and magnitudes, and the engine model that the metrics are applied to.

A notable finding in this work was the relative agreement between the Kalman filter and MAP estimator in terms of the predicted *SSEE* results and the sensor suites identified to be optimal. As previously noted, this is not unexpected given that both estimators are set up to minimize mean squared estimation error and, in the given example application, both incorporate the same *a priori* knowledge regarding health parameter covariance and sensor measurement noise covariance. However, an advantage of the MAP estimator metric is that it offers a closed-form solution while the Kalman filter *SSEE* metric requires solution of the V^* transformation matrix via an optimal iterative search. As such, the Kalman filter metric can be prone to convergence to local minima. To guard against such occurrences, a recommended approach is to cross-check Kalman filter results using the MAP metric to ensure that similar sensor suites and *SSEE* values are predicted.

The performance estimation metrics exhibited very good agreement between their theoretically predicted estimation accuracy and that obtained via Monte Carlo simulation analysis. However, the theoretical gas path fault diagnostic metric was found to underpredict the CCR found via Monte Carlo analysis. This is due to the two-fault class misclassification assumption made in deriving the metric.

While this simplification does make the derivation tractable, it can lead to inaccurate results, especially when faults are prone to misclassification as more than one fault type. Another simplification made in this derivation is to assume that all sensor residual measurements are independent. This assumption does not usually hold for gas turbine engine applications, as some amount of covariance usually exists between sensor residual measurements. For example, they are corrected using the same parameters and generated using the same reference model. An approach to address this is to define sensor measurement probability density functions in multi-parameter space and then perform multidimensional integration to assess detection and classification performance. However, this would add much more complexity. The given metric based on the properties of the chi square distribution and the non-central chi square distribution is more simplistic, but should be verified by additional analysis such as the Monte Carlo simulation analysis conducted in this paper.

A couple of recommendations for follow-on work are suggested. First, the presented analytical metrics are based on linear theory while aircraft engines exhibit nonlinear behavior. As such, a recommendation to extend the analysis to full-envelope engine operation would be to repeat the analysis at different engine operating points to assess how this affects sensor selection results. Furthermore, equal importance is placed on each parameter to be estimated and each fault type to be diagnosed. A natural extension to the metrics is to place a user-specified weighting on the different parameters or faults based on their criticality or frequency of occurrence. Finally, the estimation and diagnostic accuracy is only one piece of the overall sensor selection decision process. Other factors of merit include criteria such as sensor weight, reliability, and overall life cycle cost. Those factors should also be considered as part of the sensor selection process.

Conclusions

The sensor selection metrics introduced in this paper provide analytical tools to assist engine health management system designers in making sensor selection decisions. The metrics are easy to use, and are specifically tailored towards estimation and diagnostic approaches commonly applied to aircraft engines. They can be readily applied for assessing the benefits of adding or removing currently available engine sensors, or assessing the benefits of newly developed sensors as they become available. Through Monte Carlo simulation analysis, the metrics were verified to perform well in identifying optimal sensor suites when evaluated using linear system information. For both Kalman filter and maximum *a posteriori* health parameter estimation, the corresponding sensor selection metrics were found to perform very well in satisfying their intended objective—identifying the sensor

suite that minimizes the mean sum of squared estimation errors. The gas path fault diagnostic sensor selection metric based on theoretical correct classification rate also performed well in its objective of identifying sensor suites that provide the best diagnostic performance. Due to a simplification made in the theoretical derivation, the metric was found to underpredict the true correct classification rate. However, it does provide a theoretical lower bound on correct classification performance offered by a given sensor suite. Additionally, it is effective for identifying fault pairs at risk for misclassification and making sensor selection decisions to address such risks. Recommended follow on work is to couple these accuracy metrics with additional figures of merit pertinent for sensor selection decision. This includes considering the individual criticality of the performance parameters to be estimated or the fault types to be diagnosed, and to also couple these metrics with additional metrics reflecting the life cycle cost of adding specific sensors.

References

1. Volponi, A., Wood, B., (2005), "Engine Health Management for Aircraft Propulsion Systems," The Forum on Integrated System Health Engineering and Management (ISHEM) in Aerospace, November 7-10, Napa, CA.
2. Volponi, A.J., et al., (2003), "Gas Turbine Condition Monitoring and Fault Diagnostics", Von Kármán Institute Lecture Series, VKI LS 2003-01, Rhode-Saint-Genèse, Belgium.
3. Mushini, R., Simon, D., (2005), "On Optimization of Sensor Selection for Aircraft Gas Turbine Engines," *Proceedings of the 18th International Conference on Systems Engineering (ISCEng'05)*, August 16-18.
4. Borguet, S., and Léonard, O. (2008), "The Fisher Information Matrix as a Relevant Tool for Sensor Selection in Engine Health Monitoring," *International Journal of Rotating Machinery*, Vol. 2008, Article ID 784749.
5. Sowers, T.S., Kopasakis, G., and Simon, D.L., (2008), "Application of the Systematic Sensor Selection Strategy for Turbofan Engine Diagnostics," *ASME Turbo Expo Conference*, paper ASME GT2008-50525, Berlin, Germany, June 9-13.
6. Kaboukos, P., Oikonomou, P., Stamatis, A., Mathioudakis, K., (2001), "Optimizing Diagnostic Effectiveness of Mixed Turbofans by Means of Adaptive Modelling and Choice of Appropriate Monitoring Parameters," RTO AVT Symposium on "Ageing Mechanisms and Control: Part B – Monitoring and Management of Gas Turbine Fleets for Extended Life and Reduced Costs," Manchester, UK, October 8-11.
7. Simon, D.L., and Garg, S., (2010), "Optimal Tuner Selection for Kalman Filter-Based Aircraft Engine Performance Estimation," *Journal of Engineering for Gas Turbines and Power*, Vol. 132 / 031601-1-10.
8. Simon, D.L., Garg, S., (2009), "A Systematic Approach to Sensor Selection for Aircraft Engine Health Estimation," *19th ISABE Conference (ISABE 2009) sponsored by the International Society for Air Breathing Engines*, ISABE-2009-1125, Montreal, Canada, September 7-11.
9. España, M.D., (1994), "Sensor Biases Effect on the Estimation Algorithm for Performance-Seeking Controllers," *Journal of Propulsion and Power*, Vol. 10, No. 4, pp. 527-532.
10. Doel, D.L., (1994), "An Assessment of Weighted-Least-Squares-Based Gas Path Analysis," *Journal of Engineering for Gas Turbines and Power*, Vol. 116, No. 2, pp. 366-373.
11. Abramowitz, M., Stegun, I.A., (1965), *Handbook of Mathematical Functions*, Dover Publications, New York.
12. Sorum, M.J., (1971), "Estimating the Conditional Probability of Misclassification," *Technometrics*, Vol. 13, No. 2, pp. 333-343.
13. May, R. D., Csank, J., Lavelle, T. M., Litt, J. S., and Guo, T-H., (2010), "A High-Fidelity Simulation of a Generic Commercial Aircraft Engine and Controller," AIAA-2010-6630, 46th AIAA Joint Propulsion Conference and Exhibit, Nashville, TN, July 25-28.

